Journal of Marine Research, 56, 463–487, 1998

A numerical study of layer formation due to fingers in double-diffusive convection in a vertically-bounded domain

by Tamay M. Özgökmen[1], Oleg E. Esenkov[1] and Donald B. Olson[1]

ABSTRACT

The evolution of fingers in a double-diffusive system is investigated using numerical integration of two-dimensional equations of motion for an incompressible, Boussinesq fluid. The computational domain is periodic in the horizontal direction and is closed with no-flux boundary conditions in the vertical direction. The main result of this study is the evolution of the system from initially linear profiles for both fast and slow diffusing components to a layered state characterized by a finger zone sandwiched between two mixed layers. The horizontal boundaries in this system play an important role in the development of the layered state. At the top and bottom boundaries, light and heavy finger fluxes accumulate leading to the formation of mixed layers exhibiting larger-scale eddies. In the quasi-equilibrium state, the finger zone is characterized by broken wiggly fingers which do not extend across the entire interface. The salinity flux at the mid-depth of the domain is approximately proportional to the $\frac{4}{3}$ power of the salinity difference between the mixed layers, except for the initial phase and for the run-down phase.

1. Introduction

Double-diffusive instabilities of a fluid rely on the presence of two state variables that diffuse at different rates. Salt-fingering instability can occur when the faster diffusing component makes a stabilizing contribution to the density gradient while the slower diffusing component makes a destabilizing contribution. With the overall stratification remaining stable, the structures realized are tall, narrow cells of alternately rising and sinking fluid. In the original theory and experiment performed with a heat-salt system (Stern, 1960), two orders of magnitude difference between the diffusivities of salt and heat led to the near conservation of salt in narrow columns, hence the name "salt fingers."

Laboratory experiments (e.g., Turner, 1967; Stern and Turner, 1969) demonstrate that salt fingers cannot grow indefinitely but reach a finite amplitude. This is observed to result in the formation of a number of salt-finger zones in between mixed layers in the vertical. Salt fingers not only constitute an interesting fluid dynamics problem, but also have important implications in many fields (see Turner, 1985, for a review) including oceanography. Salt fingers are observed in the Mediterranean outflow (Williams, 1974), in the North Atlantic Current (Schmitt and Georgi, 1982), and during the Caribbean-Sheet and

1. RSMAS, MPO, University of Miami, 4600 Rickenbacker Causeway, Miami, Florida, 33149, U.S.A.

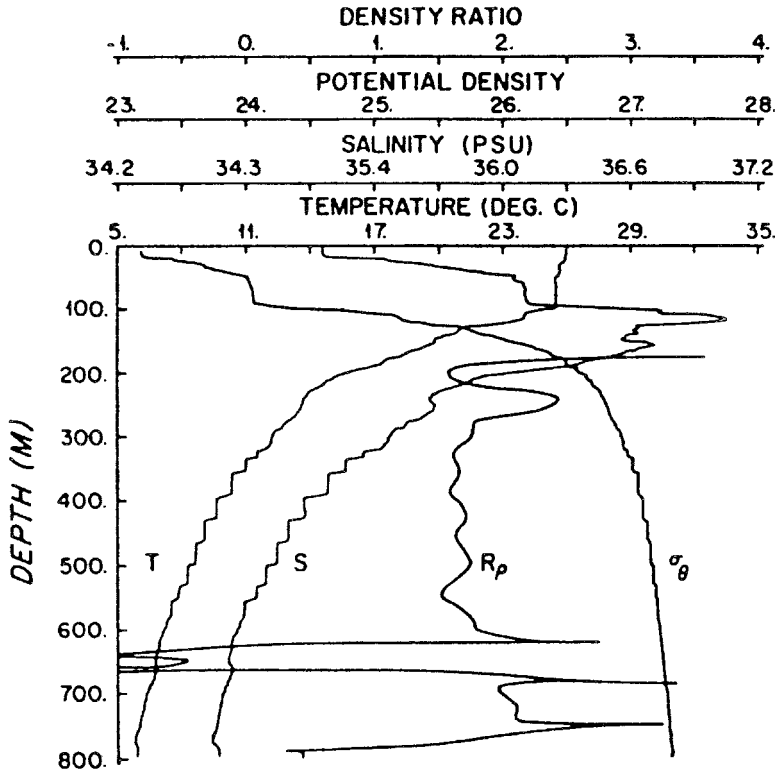

Figure 1. The vertical profiles of temperature, salinity, potential density anomaly (σ_θ), and density ratio (R_ρ) from a station in the C-SALT area (from Schmitt *et al.,* 1987).

Layers Transects (C-SALT) experiment (Schmitt *et al.,* 1987; Marmorino, 1987). All of these regions are characterized by the differential advection of warm and salty water over cold and fresh water. These observations document a finger-scale microstructure (typically few centimeters thick) that extends typically a few meters in the vertical and is separated from others by well-mixed regions (typically tens of meters thick) leading to temperature and salinity steps (Fig. 1). "Thermohaline staircases" are observed over an area of 1 million square kilometers east of Barbados. Schmitt (1981) proposes that salt fingers play an important role in determining the structure of the thermocline waters of the subtropical ocean gyres.

It is still not clearly understood what mechanisms limit the growth of fingers and determine the vertical extent and vertical structure of the salt-finger zones. Stern (1969) investigates the stability of long, steady, two-dimensional salt fingers to long-wavelength internal wave perturbations. He shows that if the fluxes through the fingers are large enough, then the fingers become unstable. This theory is known as the collective instability of salt fingers. The term 'collective instability' refers to the transfer of energy to relatively larger-scale perturbations by means of the cumulative stress exerted by a group of salt

fingers moving together. According to this theory, fingers cease to grow when the shear associated with the large-scale motion is sufficient to disrupt the fingers. Alternatively, Kunze (1987) uses a Richardson number constraint to limit the length and fluxes of the fingers, and shows that this constraint is equivalent to the collective instability criterion. However, direct numerical simulations of finger convection by Shen (1989) do not substantiate step formation and the collective instability theory for a low Prandtl number fluid (i.e., for Prandtl numbers between 1 and 10). Holyer (1984) considers the stability of long, steady, two-dimensional fingers to perturbations of all wavelengths. Holyer (1984) suggests that collective instability is only dominant at large Prandtl numbers (i.e., for Prandtl numbers greater than 1000), and proposes another kind of instability, which starts to grow between the fingers where the shear is maximum. It is argued in Holyer (1984) that this instability could be responsible for limiting the length of fingers in a low Prandtl number system, such as the heat-salt system. The focus of many previous studies has been on the initial evolution of the fingers, and on the idealized case of infinite fingers where the variability in the vertical direction is neglected, while the formation of the mixed layers and their interaction with the finger zone is not completely understood.

Here, the purpose is to simulate the evolution of fingers to a finite amplitude, and the subsequent formation of mixed layers, by employing numerical integration of two-dimensional equations of motion. The coupling between different length and time scales is extremely difficult to explore using analytical techniques. In many previous numerical studies (Piacsek and Toomre, 1980; Shen, 1989, 1993), the initial configuration corresponds to two mixed layers separated by a sharp interface. Whitfield *et al.* (1989) conduct experiments where steplike temperature and salinity perturbations are superimposed on constant, uniform background gradients. Shen and Veronis (1997) perform high-resolution numerical experiments where larger-scale eddies form in the reservoirs, but an equilibrium is not reached. In the present study, the experiment is initialized with uniform vertical gradients for both slow and fast diffusing components, and the fully nonlinear equations are solved. It is demonstrated that the simulation captures some characteristics observed in laboratory experiments. Most importantly, the system evolves to a quasi-equilibrium state characterized by a finger interface in between two mixed layers.

The paper is organized as follows: the numerical model is introduced in Section 2. In Section 3, considerations leading to the experiment are discussed. The evolution of the numerical simulation is presented and analyzed in Section 4. The results are discussed in Section 5 and summarized in the concluding section.

2. The numerical model

The numerical model integrates the two-dimensional equations of motion of an incompressible fluid subject to the Boussinesq approximation. In this study, the fast-diffusing component is referred to as T or 'T-stuff,' and the slow-diffusing component as S or

'*S*-stuff' (after Stern and Turner, 1969). In order to reduce the number of parameters, the following nondimensionalization is used:

$$(x, z) = L(x^*, z^*);\ \psi = \nu\psi^*;\ t = \frac{L^2}{\nu}\, t^*;\ T = \Delta T\, T^*;\ S = \Delta S\, S^*.$$

Dropping stars, the prognostic equations for the conservation of vorticity, *T*-stuff, and *S*-stuff become

$$\zeta_t + J(\psi, \zeta) = \frac{Ra}{Pr}\left(T_x - \frac{S_x}{R_\rho}\right) + \nabla^2\zeta, \tag{1}$$

$$T_t + J(\psi, T) = \frac{1}{Pr}\nabla^2 T, \tag{2}$$

$$S_t + J(\psi, S) = \frac{1}{Sc}\nabla^2 S. \tag{3}$$

The streamfunction is calculated diagnostically from

$$\nabla^2\psi = \zeta. \tag{4}$$

Here ν is the kinematic viscosity, K_T and K_S are the respective diffusivities of *T*-stuff and *S*-stuff, ΔT and ΔS are the respective *T* and *S* differences across the vertical extent of the domain, g is the gravitational acceleration, and L is the width of the domain. A linear equation of state is employed where α and β are the expansion coefficients for *T* and *S*, respectively. The nondimensional parameters are the density ratio $R_\rho = \alpha\Delta T/\beta\Delta S$, Prandtl number $Pr = \nu/K_T$, Schmidt number $Sc = \nu/K_S$, and Rayleigh number based on *T*-stuff $Ra = g\alpha\Delta T L^3/\nu K_T$.

The prognostic equations, (1)–(3), are advanced in time using a predictor-corrector type explicit leapfrog method which is fully corrected against numerical instabilities (Gazdag, 1976). The time step is calculated at every iteration based on the maximum speed induced by diffusive and advective processes. The Jacobian operator $J(a, b) = a_x b_z - a_z b_x$ is computed using the formulation proposed by Arakawa (1966) that conserves kinetic energy and enstrophy, while accurately maintaining the property $J(a, b) = -J(b, a)$. The diagnostic equation, (4), is inverted using a Fast Fourier Transform solver (Swarztrauber, 1977).

3. Experimental considerations

Oceanic observations (e.g., Williams, 1974; Marmorino, 1987) have revealed finger-like laminae of centimeter scale, finger zones or interfaces that range from tens of centimeters to a few meters, and mixed layers typically tens of meters thick. Since the scales for fingers, interfaces and layers differ by orders of magnitude, one of the main challenges facing a numerical experiment of this type is the difficulty of capturing such a wide spectrum of scales within the model domain. Salt fingers must be 'adequately' resolved while

considering limitations regarding the overall integration time, given the available computer resources. One of the choices made in this study is to focus on salt fingers while capturing a portion of the layers on each side of the finger zone, rather than trying to resolve multiple layering. The primary purpose is to simulate the evolution of a finger zone and layers from constant-gradient stratification using the most convenient values of parameters. Since the layer and interface thicknesses are functions of Pr and Sc (e.g., Stern, 1969), these parameters can be chosen so that: (i) a salt-fingering interface sandwiched between two layers is captured and covers a large part of the model domain; (ii) the ratio of finger scale over interface thickness is large enough so that the individual fingers are adequately resolved by the numerical grid; and (iii) the number of computational iterations required for the development of the layers is as small as possible. The formulae derived in Stern (1969) are used as guidelines to determine the model parameters. Nondimensionally, these relations are (assuming that the finger zone covers the entire vertical extent of the domain):

$$\frac{d}{L} \sim Ra^{-1/4}(L_z/L)^{1/4}, \tag{5}$$

$$\frac{h}{L} \sim \left(\frac{Pr^4}{Ra\,Sc}\frac{L_z}{L}\right)^{1/4}, \tag{6}$$

$$\frac{H}{L} \sim \left(\frac{Pr^4 Sc^3}{Ra}\frac{L_z}{L}\right)^{1/4}, \tag{7}$$

where d indicates the scale for finger width, h the interface thickness, H the mixed layer thickness, and L_z is the vertical dimension of the domain. It should be noted that the above equations are order of magnitude approximations. Therefore, prior to the final simulation, the actual behavior of the system was investigated in a series of low-resolution experiments (not presented). The vertical extent of the domain is an important parameter. If the vertical domain size is 'too short,' the fingers fill the entire domain and no space is left for the development of mixed layers. On the other hand, if the domain is 'too tall' (but not tall enough to allow multiple layering), the salt-finger zone is only a small portion of the domain and mixed layers cover the rest. In this case, an excessive number of grid points and added space result in a high computational load. A high Pr number results in a slow development of the fingers that can be interpreted as being due to slow diffusion of T-stuff or high viscous damping. For instance, the salt-sugar system, which has been commonly employed in laboratory experiments because of its advantages during initial experimental setup, was prohibitively slow to evolve in preliminary numerical experiments because of the very high Pr number ($Pr = 1000$). On the other hand, a low Pr number leads to a fast development of fingers that quickly become unstable and display a transition to turbulence. Despite its relevance to oceanic observations, the heat-salt system ($Pr = 7$) is numerically quite challenging because of its demand on resolution due to turbulence and a very sharp interface [Eq. (6)]. Also, a low K_T/K_S (i.e., $O(1)$) is desirable because boundary layers of

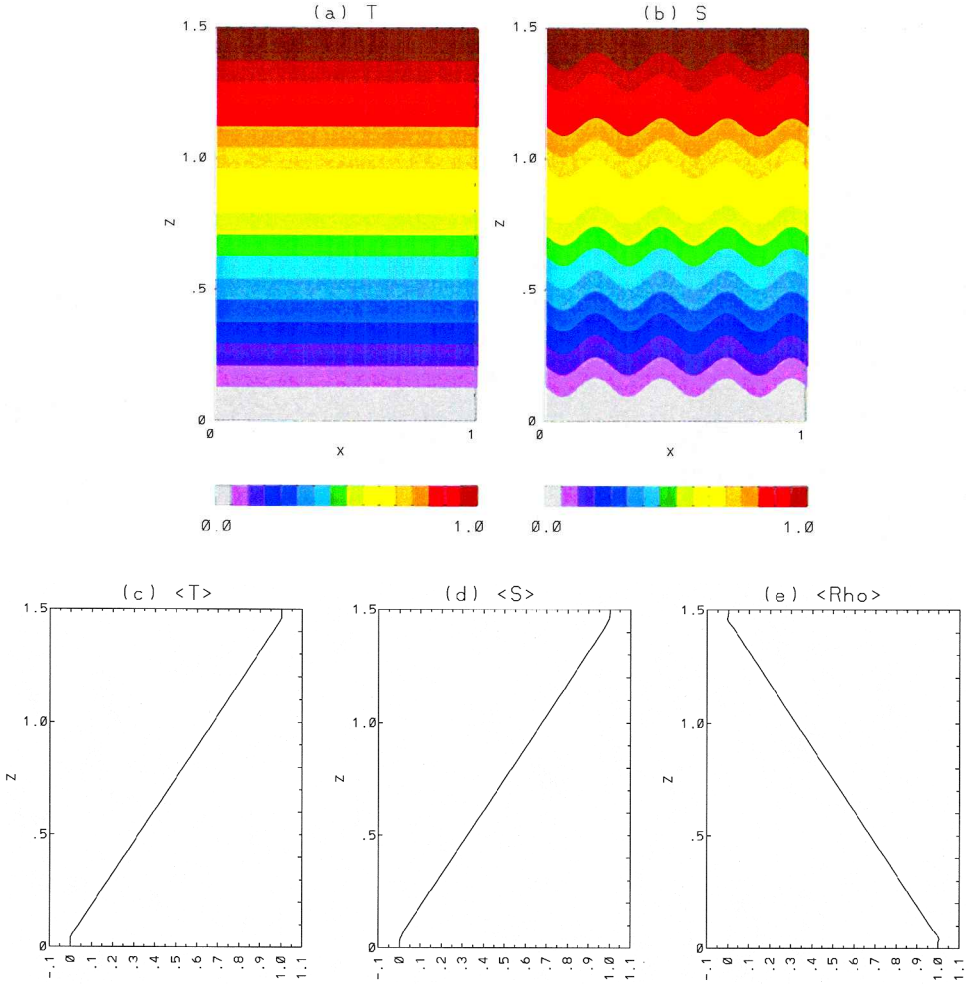

Figure 2. Model initial conditions for (a) $T(x, z)$ and (b) $S(x, z)$. Resulting vertical profiles of (c) T-stuff, (d) S-stuff and (e) density. For the purpose of plotting, density is defined as $\rho = 1 - (R_\rho T - S)/(R_\rho - 1)$ so that it varies from 0 to 1 as T and S vary from 1 to 0. The script $\langle T \rangle$ denotes the horizontal average of $T(x, z)$.

S-stuff cannot otherwise be resolved, even if boundary layers of T-stuff are adequately resolved. However, even though salt fingers can develop with very low K_T/K_S, such as the salt-sugar system ($K_T/K_S = 3$), a small difference between the diffusivities leads to a slow evolution.

Based on the above considerations and preliminary results from low-resolution test cases, Pr and Sc numbers are selected that lie between salt-sugar ($Pr = 1000$, $K_T/K_S = 3$) and heat-salt systems ($Pr = 7$, $K_T/K_S = 100$). In the double-diffusion experiment presented here $Pr = 100$ and $Sc = 3000$ (hence, $K_T/K_S = 30$). Physically, this system

corresponds to double-diffusive convection of starch and sugar in water, but it is not known whether any laboratory experiments involving these two components exist.

The requirement for salt-finger instability is

$$1 < R_\rho < K_T/K_S. \tag{8}$$

Here, the initial density ratio is taken as $R_\rho = 1.6$, and since $K_T/K_S = 30$ the above requirement is satisfied. It is anticipated that a small density ratio (i.e., $R_\rho \to 1$) will result in a faster development of fingers than a large density ratio (i.e., $R_\rho \to K_T/K_S$) because the former is gravitationally less stable.

The integrations are carried out in a rectangular domain with an aspect ratio of $L_z/L = \frac{1}{2}$. The boundary conditions on the lateral sides (i.e., left/right) are periodic. At the top and bottom, the boundary conditions are free-slip and no vertical mass flux ($\zeta = 0$, $\psi_x = 0$). Furthermore, no T and S fluxes are allowed across these boundaries (i.e., $T_z = 0$, $S_z = 0$). Unlike periodic or Dirichlet boundaries, this condition does not drive the system through fluxes which are determined via feedback between the internal system and the boundaries. Such fluxes can 'heat' or 'cool' the system from the top or bottom, greatly modifying the nature of the problem we are interested in exploring. It is anticipated that no-flux boundary conditions will result in less interference with the internal system than many other possible choices, except for some kind of open boundary conditions, which are not implemented in order to keep the simulation as simple as possible.

The Rayleigh number is $Ra = 6 \times 10^7$. It is an important parameter controlling the thickness of the interface as well as the horizontal scale of fingers [Eqs. (5)–(6)]. High Ra leads to a fast evolution of the system via strong forcing. On the other hand, the finger scale gets progressively finer with increasing Ra, making its resolution computationally more demanding. The governing criteria in selecting this parameter were: (i) fingers developing from the initial conditions are resolved with 10 grid points or more in the horizontal direction, and (ii) the interface fits into the model domain and is adequately resolved.

The numerical discretization of the domain consists of 301×113 points in x- and z-directions, respectively ($\Delta z \approx 4\Delta x$ in order to take advantage of the 'finger' shape). The main computational load is due to separation of time scales between fast finger growth and slow large-scale evolution, which required approximately 2×10^6 iterations and took about two weeks to run on a 275 MHz Alpha/DEC workstation. (The nondimensional time step is typically $\Delta t \approx 1 \times 10^{-6}$ for the present experiment.) Since doubling the resolution in each coordinate direction increases the computation time approximately by an order of magnitude, the present resolution is the highest that can be reasonably employed given the computer resources available to us at the present time.

4. Numerical results

a. Formation of layers from constant-gradient stratification

The model integration is initialized with the T and S fields shown in Figure 2a and b. The fields consist of constant-gradient distributions over the vertical extent of the domain such

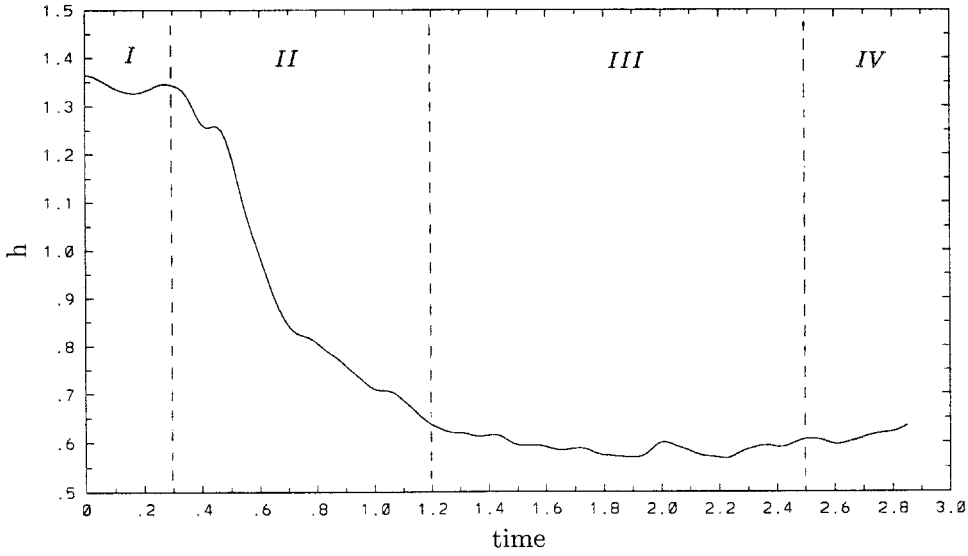

Figure 3. Evolution of interface thickness h throughout the integration.

that the T-profile is stabilizing and the S-profile destabilizing (Figure 2c,d), consistent with the requirement for finger instability. Near the horizontal boundaries, narrow zones with zero gradient are specified so that the boundary conditions for T and S are satisfied. The overall stratification is gravitationally stable (Fig. 2e) since $R_\rho > 1$. In order to facilitate the development of fingers, sinusoidal perturbations are superimposed on the S field (Fig. 2b). The wavelength of these perturbations is larger than the finger scale based on the initial Ra. Alternatively, random perturbations can be used. The purpose of these perturbations is to reduce the total integration time by speeding up the initial onset of finger instability. The evolution of the system is otherwise not sensitive to these perturbations.

The finger zone is the stratified region sandwiched between two mixed layers. Here, the edge of the interface is defined where the density gradient exceeds an empirically determined value. The density gradient of the initial stratification is $\rho_z^0 \approx \Delta\rho^0/L_z = -1/(3) = -\frac{2}{3}$, where $\Delta\rho^0$ is the initial density difference across the vertical extent of the domain. The interface is specified as the region where the density gradient $\rho_z < -\frac{1}{3}$. The qualitative behavior of the interface thickness seems to be well captured by this definition, because it does not show much sensitivity to other selections of a density gradient around this value. Evolution of the interface thickness h based on this definition is demonstrated in Figure 3. Its behavior can be split roughly into four distinct regimes: (I) initial phase where h remains approximately constant ($0 < t < 0.3$); (II) followed by a period where the interface thickness decreases ($0.3 < t < 1.2$); (III) a quasi-equilibrium state at minimum h ($1.2 < t < 2.5$); and (IV) the 'run-down' phase where the interface starts expanding ($t > 2.5$).

Initially, h is slightly less than the total vertical extent of the domain due to the presence

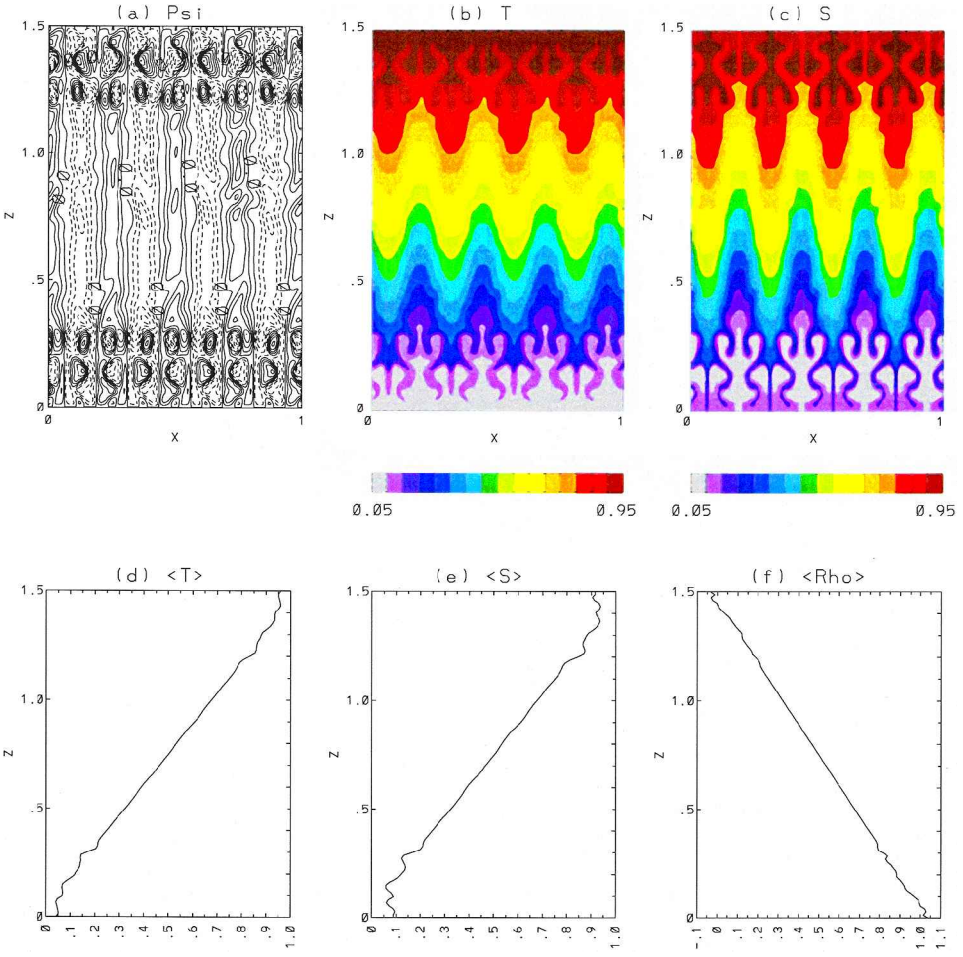

Figure 4. (a) $\psi(x, z)$ (CI = 0.03), (b) $T(x, z)$, (c) $S(x, z)$ and vertical profiles of (d) T-stuff, (e) S-stuff and (f) density at $t = 0.3$.

of narrow buffer zones near the boundaries. Phase I is characterized by diffusive processes. The interface thickness does not display any significant change until fingers start developing from the initial stratification. The state of the system at the end of this phase (at $t = 0.3$ or after 2.2×10^5 iterations) is illustrated in Figure 4. Quasi-laminar, finger-scale motion is evident near the horizontal boundaries. The initial vertical profiles of T and S are nonuniform near the horizontal boundaries, where no-flux conditions are imposed. Due to the change of the gradient in the profiles near the horizontal boundaries, such locations are prone to faster diffusion. Hence, the T profile is smoothed by diffusion whereas the S profile remains roughly the same, decreasing the local density ratio. A smaller density ratio is associated with less gravitational stability, leading to faster development of fingers near the

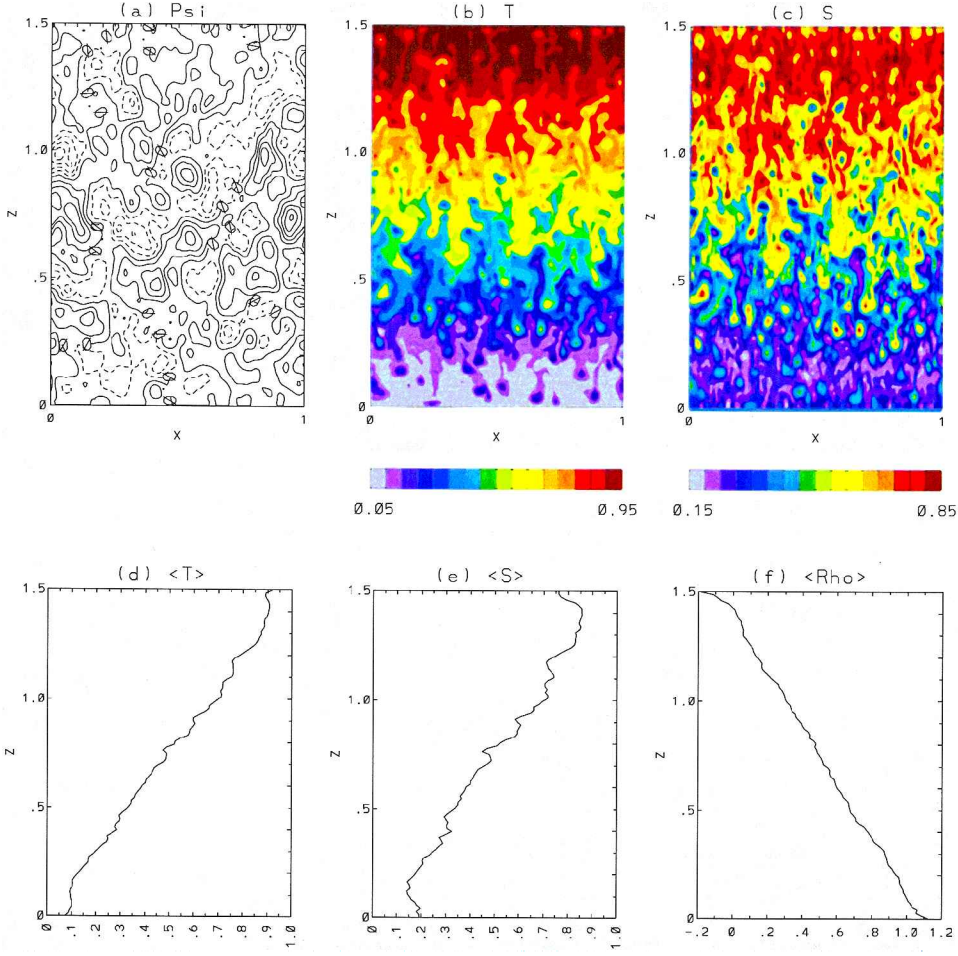

Figure 5. (a) $\psi(x, z)$ (CI = 0.3), (b) $T(x, z)$, (c) $S(x, z)$ and vertical profiles of (d) T-stuff, (e) S-stuff and (f) density at $t = 0.5$.

horizontal boundaries. Some perturbations start to grow also near mid-depth as seen in the streamfunction plot (Fig. 4a). These perturbations display a fast growth in Phase II. The state of the calculated fields at $t = 0.5$ is shown in Figure 5. At this instant, finger-scale activity fills the entire domain (Figs. 5a,b,c). There is little indication of layering or any scale separation between fingers and a larger-scale flow at this time. Fingers transports properties (primarily S-stuff) in both vertical directions. Consequently, density exceeds its original limits (0 to 1) near the horizontal boundaries (Fig. 5f). It is worth noting that individual fingers do not extend across the entire vertical extent of the domain during this phase.

Figure 6 illustrates the state of the system at $t = 1.7$, representing the quasi-equilibrium state during phase III. The finger zone now appears to be sandwiched between two layers

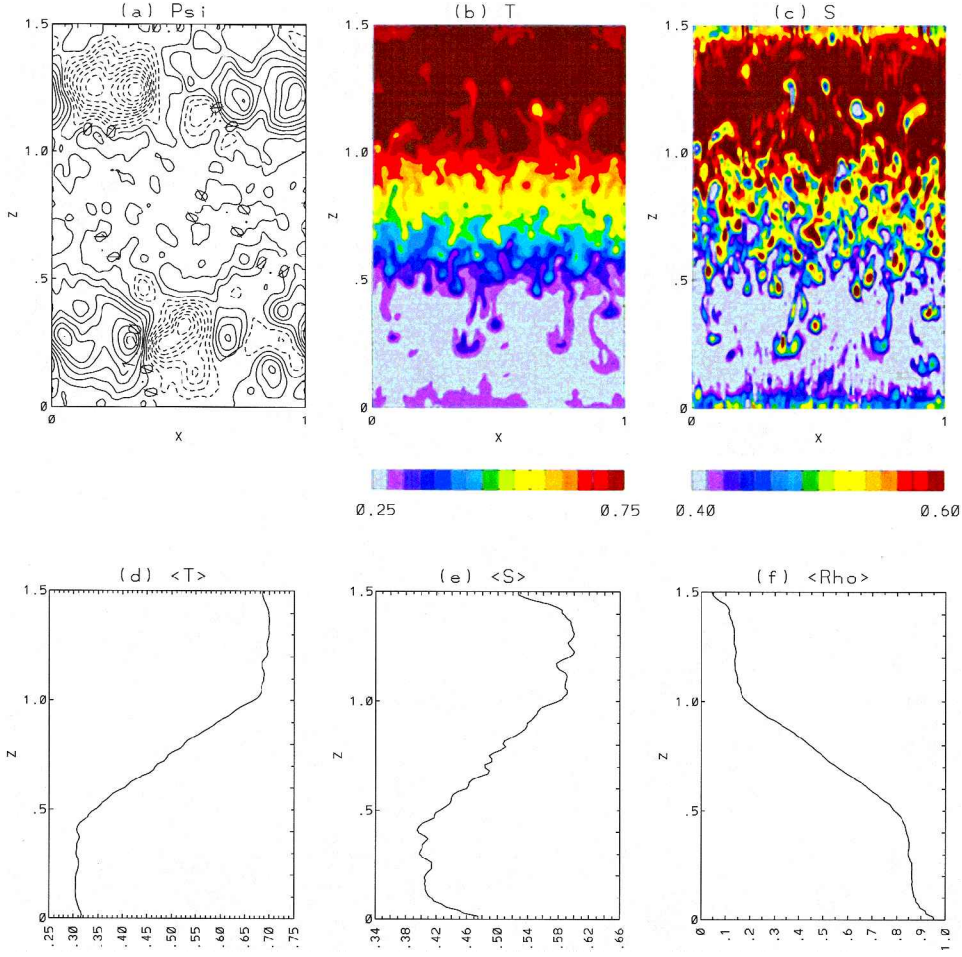

Figure 6. (a) $\psi(x, z)$ (CI = 0.3), (b) $T(x, z)$, (c) $S(x, z)$ and vertical profiles of (d) T-stuff, (e) S-stuff and (f) density at $t = 1.7$.

where the properties are constant in the statistical sense. Step formation is clearly visible in all profiles (Fig. 6d,e,f). At the edge of the finger zone blobs become unstable and break away. Some fingers extend well into the mixed layers (Fig. 6b,c). The buoyancy of these convective elements is dominated by S-stuff anomaly. Figure 6c illustrates that finger activity transfers salinity between the layers. The flow pattern in mixed layers is illustrated in Figure 6a, which indicates that the motion there consists of larger-scale cells. Due to strong convection, the vertical density profile shows an approximately neutral stratification in the mean (Fig. 6f). The flow in the finger zone is visualized by plotting the velocity field $(u, w) = (-\psi_z, \psi_x)$ for $0.3 < z < 1.2$ (Fig. 7). The finger zone is characterized by alternately rising and sinking motions. The fingers do not extend across the interface as

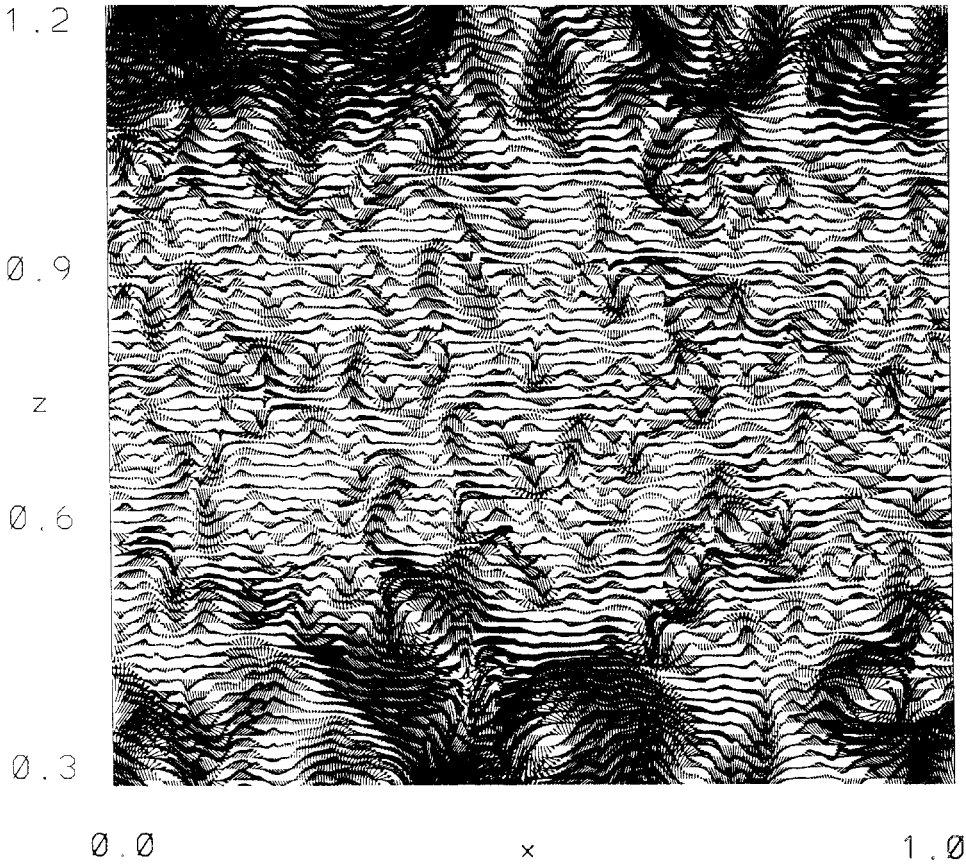

Figure 7. The velocity field for $0.3 < z < 1.2$ at $t = 1.7$.

continuous columns of fluid, but still exhibit an aspect ratio (length over width), which is generally larger than unity. There is a pronounced shear in the transition zone from the finger region to the layers. The simulated fingers are not purely vertical and quasi-laminar as in laboratory experiments conducted primarily with heat-salt or sugar-salt systems. This could be an artifact of the parameter choices. However, recent laboratory experiments by Taylor and Buchens (1989) exhibit heat-salt fingers which are also highly irregular and spatially nonuniform.

The *S* field in the present experiment shows some boundary effects (Fig. 6c,e). This is because blobs with low *S*-stuff in the upper reservoir (and vice versa) do not have enough vertical space to completely mix before reaching the no-flow boundary. As a consequence, they tend to accumulate along the horizontal boundaries. On the other hand, *T*-stuff is completely mixed in these layers because of its higher diffusivity.

Toward the end of the integration (Phase IV), the finger zone exhibits signs of slow expansion. Fingers convert potential energy available in the *S*-stuff distribution to kinetic

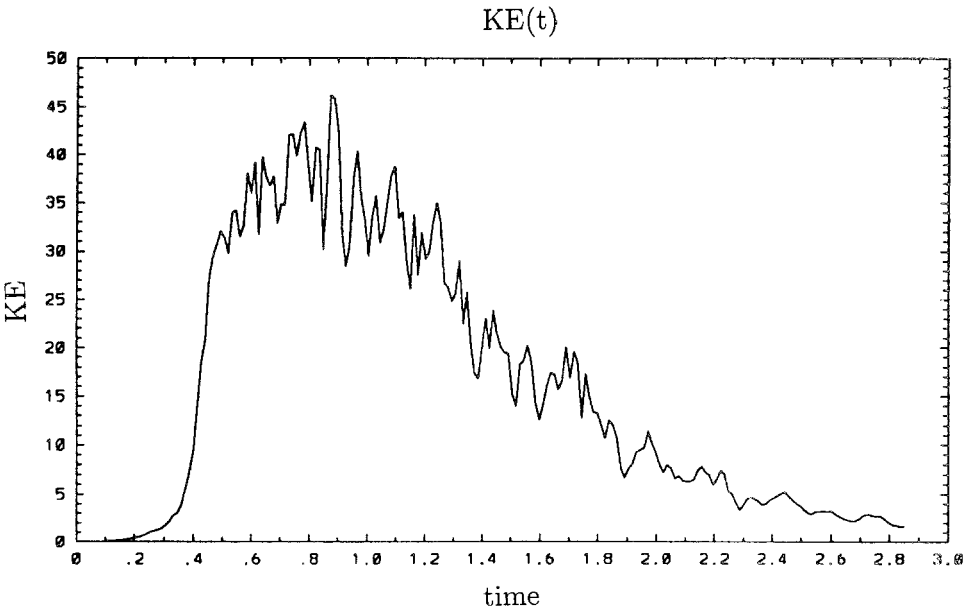

Figure 8. Evolution of basin-integrated kinetic energy.

energy, which is then dissipated by viscosity. Given that the vertical extent of the domain is limited and the horizontal boundaries do not allow for T or S fluxes, the available potential energy maintaining the finger convection reduces after a certain time, leading to the decay of the layered state. A similar decay of the interface is observed in laboratory experiments (e.g., Stern and Turner, 1969). As the fingers feed on the potential energy available in the S-stuff distribution, the S-stuff difference between the mixed layers decreases. Finger convection driven by the slow diffusing component (S) weakens, hence the rate of potential energy release decreases and the convective cells weaken. Consequently, the interface starts to expand due to the vertical diffusion of T. Since the primary interest in this paper is in the phase where a balance is sustained between the finger zone and mixed layers, the numerical integration was terminated when the onset of the 'run-down' phase became evident. The reader is referred to Shen (1989) for a detailed discussion of this phase.

The evolution of basin-averaged kinetic energy is illustrated in Figure 8. The initial rapid growth of kinetic energy due to finger instability is followed by gradual decay when the motions in the finger zone and in the mixed layers weaken.

Figure 9 demonstrates the evolution of the difference of T and S between layers, and their vertical gradients at mid-depth ($z = 0.75$) throughout the integration. As explained above, the S-stuff difference reduces continuously because of advective transfer between layers (Fig. 9b). On the other hand, diffusive effects dominate in the case of T-stuff. The equilibrium in Figure 9a indicates that by the time a water parcel with low T-stuff is transferred to the upper reservoir, it has almost 'warmed' up to the temperature of the upper

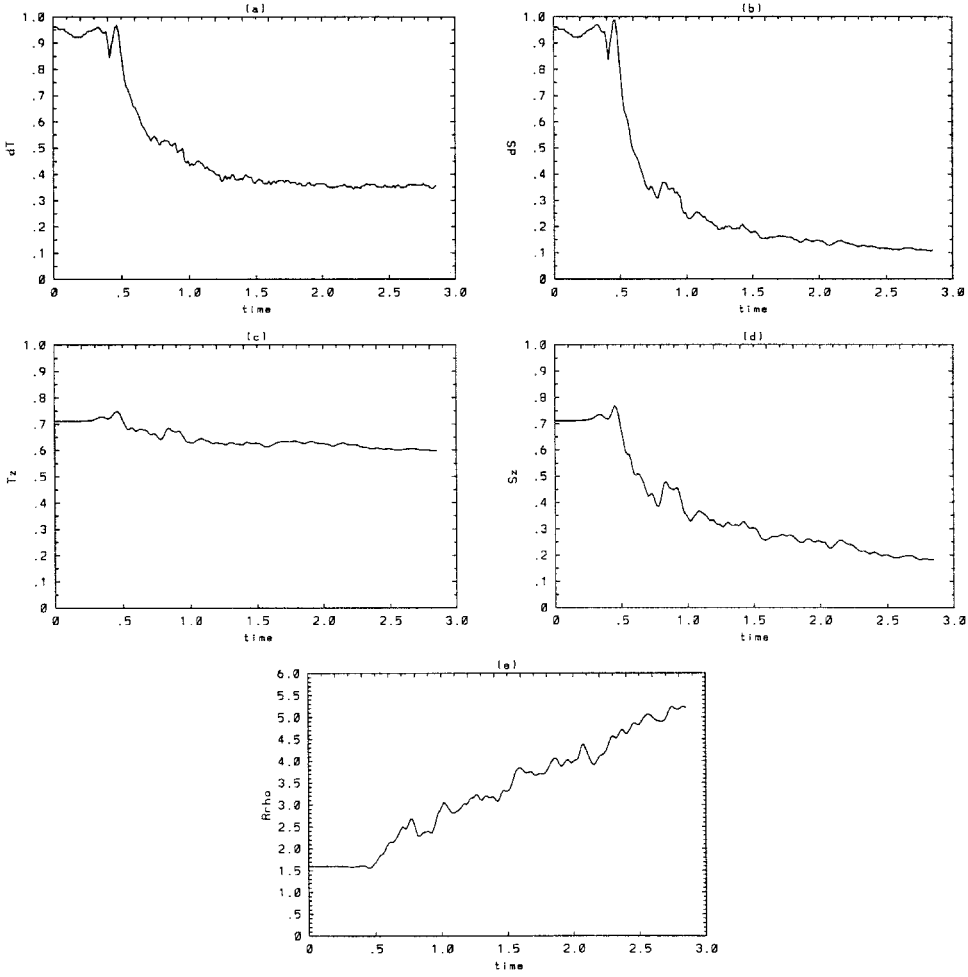

Figure 9. Evolution of (a) the difference in T-stuff between layers, (b) the difference in S-stuff between layers, (c) $\langle T \rangle_z$ at mid-depth ($z = 0.75$), (d) $\langle S \rangle_z$ at mid-depth and (e) density ratio R_ρ throughout the integration.

reservoir (and vice versa). Consequently, the stabilizing component (T) maintains an equilibrium difference, whereas the destabilizing component (S) is mixed in the vertical by finger convection. Hence, the system becomes gravitationally more stable as time progresses (Fig. 9e).

b. Finger structure and numerical accuracy

Finger profiles are explored in more detail by plotting the variations in S-stuff, T-stuff, and vertical velocity in the finger zone. In order to remove the background stratification, we define $S' = S - \langle S \rangle$ and $T' = T - \langle T \rangle$, where S' and T' are the fluctuations about the

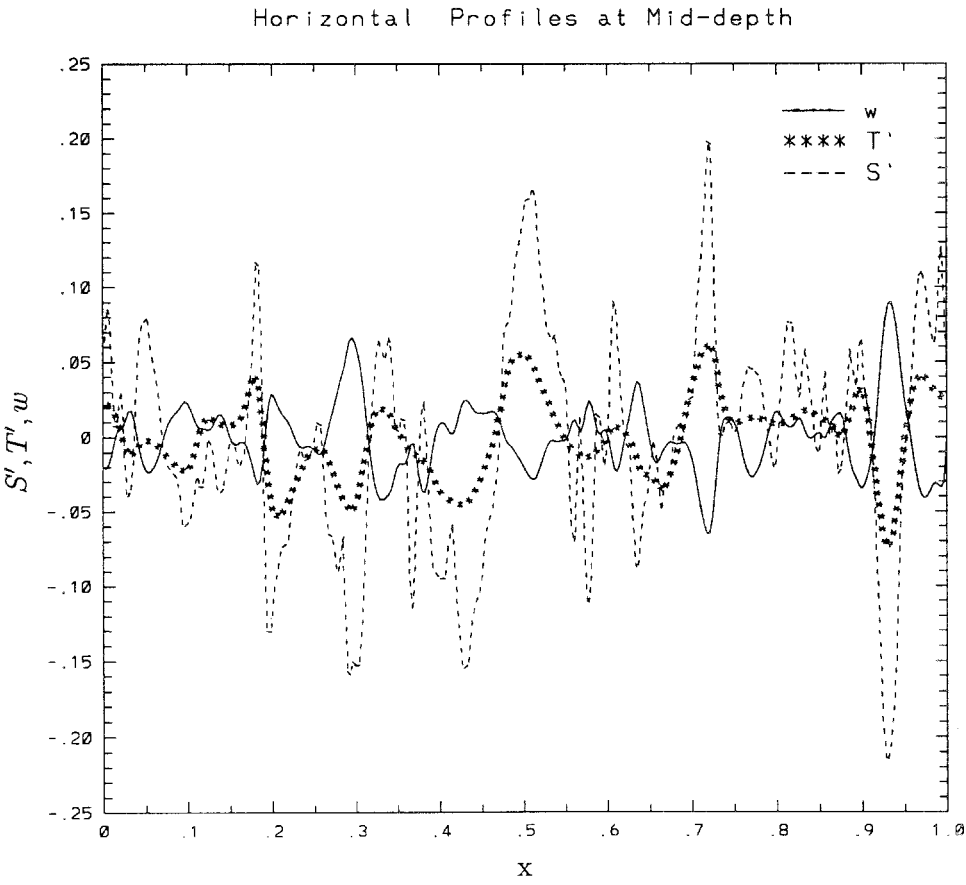

Figure 10. Horizontal profiles of T', S' and w along mid-depth of the domain ($z = 0.75$) at $t = 1.7$. Vertical velocity w is scaled by 100.

horizontal means $\langle S \rangle$ and $\langle T \rangle$. The profiles along the mid-depth of the domain ($z = 0.75$) at $t = 1.7$ are shown in Figure 10. This graph indicates upward (downward) transfer of negative/"colder and fresher" (positive/"warmer and saltier") T and S anomalies. The number of groups of rising and sinking fingers indicated by this graph is around 10. The profiles for vertical velocity (see also Fig. 7) and T' exhibit smooth variations, which indicate that these fields can be considered as adequately resolved. The salinity profiles exhibit a somewhat noisy structure.

The fluctuations inside finger groups could be associated with slower-growing finger modes as well as numerical instability. Therefore, the limitations of the numerical resolution of the fingers should be clarified. The following relationships can be written for a convective motion described by Eqs. (1)–(3) (e.g., Shen, 1989): $\delta_v/\delta_T = \sqrt{Pr}$ and $\delta_S/\delta_T = \sqrt{Pr/Sc}$, where δ_v, δ_T and δ_S indicate the scales for viscous, temperature, and salinity diffusive scales, respectively. The finger scale is given by (Kunze, 1987): $d/L = 2\pi[Ra$

$(L/h)[1 - (1/R_\rho)]^{-1/4}$. Taking the scale for the temperature boundary layer as: $\delta_T/L = \sqrt{2}$ $[Ra(L/h)]^{-1/4}$ (c.f. Howard and Veronis, 1987), the ratio of temperature boundary layer to finger scale becomes: $\delta_T/d = (1/\sqrt{2\pi})\,[1 - (1/R_\rho)]^{1/4}$. Hence, $\delta_T/d \approx 0.2$ over the range of density ratios observed in our numerical experiment ($1.6 \leq R_\rho < 5.5$, Fig. 9e). Considering that the fingers are resolved by 10–15 grid points on average (see Fig. 7, and also from the above equation), and using the above relationships, we conclude that the viscous boundary layers are fully resolved [since $\delta_\nu/d \sim O(1)$], the temperature boundary layers are resolved typically by 2 grid points or so, but the salinity boundary layer scale corresponds to approximately half the grid spacing in the horizontal direction. The salinity boundary layers are therefore not adequately resolved.

The numerical accuracy of the present simulation is further investigated by inspecting the spectral density of the computed fields. Herring *et al.* (1974) concludes that the accuracy of the computed fields is assured if the spectral density of these fields decreases systematically with increasing wavenumber. The wavenumber spectra for S' and T' corresponding to Figure 10 are illustrated in Figure 11. The fields exhibit a general decline with increasing wavenumbers. The spectrum of S' reflects the resolution limitations of this simulation.

The sensitivity of the evolution of the system to the numerical resolution is investigated by conducting lower resolution runs, and with different aspect ratios of the grid spacings in the x- and z-directions (not shown). The formation of the mixed layers, convective cells, the thickness of the finger interface are in qualitative agreement with the present simulation.

c. On the stability of fingers

Probably the most crucial aspect of layer formation by fingers is exploring the circumstances that cause the fingers to become unstable and break up into blobs. In an attempt to explain the disruption of finger growth, Stern (1969, 1975) investigates the stability of salt fingers to long wavelength internal wave perturbations. He assumes long, steady, two-dimensional salt fingers and shows that fingers become unstable if (in dimensional form)

$$A = \frac{\beta F_S - \alpha F_T}{\nu(\alpha \langle T \rangle_z - \beta \langle S \rangle_z)} > 1, \tag{9}$$

where $F_S = \langle wS' \rangle$ and $F_T = \langle wT' \rangle$ are vertical convective fluxes of S-stuff and T-stuff. Hence, the Stern number, or the collective instability criterion A, is the ratio of the total buoyancy flux to the vertical density gradient, nondimensionalized by the viscosity. Holyer (1981) refines Stern's calculations by relaxing the assumption that the magnitude of the fluxes remains constant, and shows that fingers in a high Prandtl number fluid become unstable if the Stern number exceeds ⅓. Laboratory experiments indicate a wide range of values of A. For sugar-salt fingers, the documented values differ by several orders of

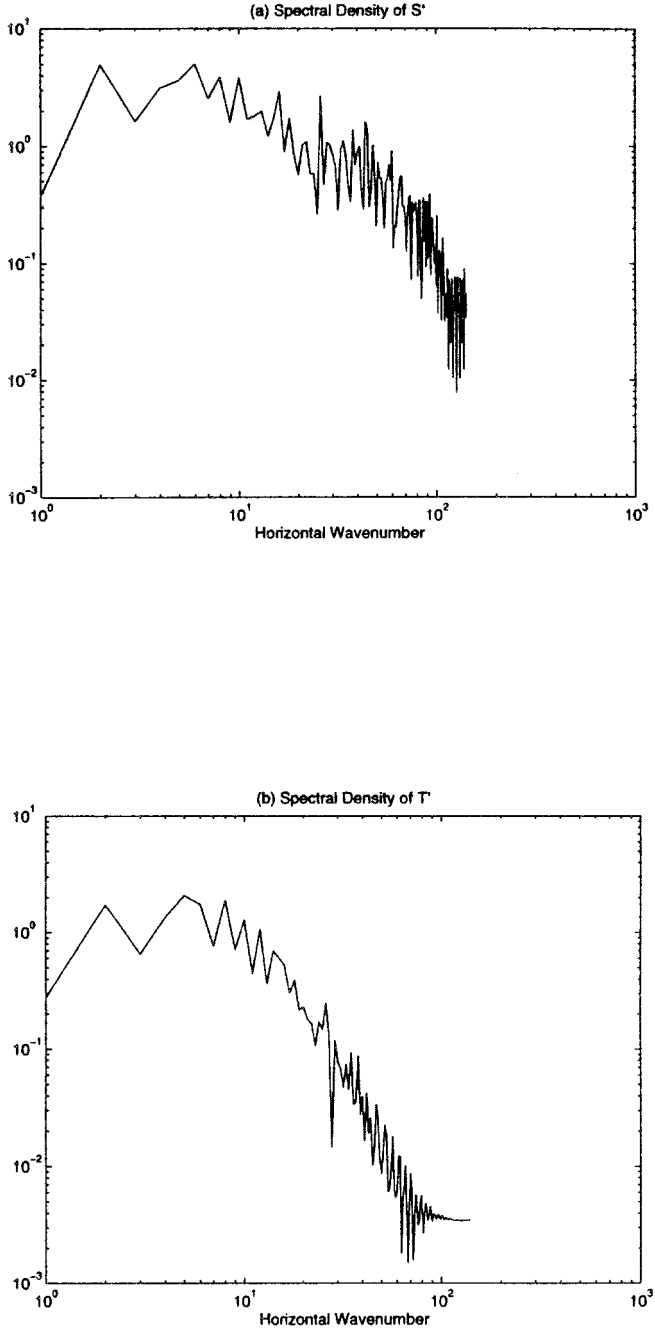

Figure 11. Horizontal wavenumber spectra for (a) S' and (b) T' along mid-depth of the domain ($z = 0.75$) at $t = 1.7$.

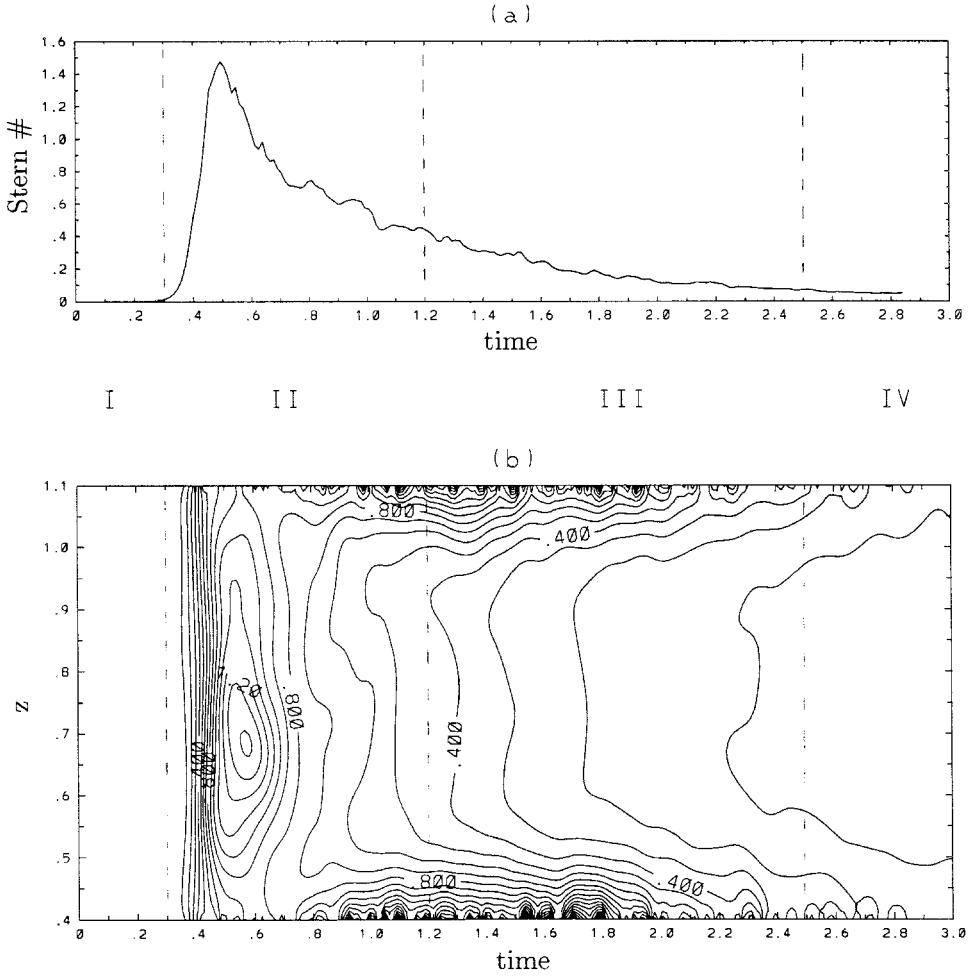

Figure 12. Evolution of the Stern number (a) at mid-depth ($z = 0.75$) and (b) across the finger zone ($0.4 \leq z \leq 1.1$).

magnitude: 0.002, Lambert and Demenkow (1972); 0.02, Griffiths and Ruddick (1980); 1–4, Stern and Turner (1969), Linden (1973).

The evolution of the Stern number at mid-depth in the present experiment is shown in Figure 12a. The Stern number increases rapidly in Phase II, and drops sharply after exceeding a value of about 1.4. This period coincides with the formation of mixed layers. During the quasi-equilibrium state (Phase III), the Stern number gradually declines from 0.45 to values lower than 0.1. Figure 12b illustrates how the Stern number evolves in time and space (vertical extent of the domain shown ranges from $z = 0.4$ to $z = 1.1$). In the quasi-equilibrium state, the Stern number is uniform in the vertical over the finger zone,

and increases rapidly in the mixed layers, making a clear distinction between the different regions.

While the Stern number provides a convenient characterization of the fingering system, it is not clear that it is the criterion controlling the stability of the fingers, because broken wiggly fingers are observed in all phases of the simulation. More recent finger instability theories by Holyer (1984), Howard and Veronis (1992) show that fingers are intrinsically unstable virtually at all scales. Considering the assumptions made in finger instability theories (infinite fingers, absence of blobs) it is hard to identify the exact nature of the instability in this simulation.

d. Fluxes

The flux ratio, R_f, defined as

$$R_f = \frac{\alpha F_T}{\beta F_S} \tag{10}$$

is the ratio of potential energy gained by the T field to potential energy lost by the S field. It must be less than unity, since otherwise the system would be gaining energy. This ratio has been the focus of many previous studies. The values of R_f obtained in laboratory experiments for heat-salt fingers vary considerably, from 0.4 to 0.8, in experiments carried out by Turner (1967), Schmitt (1979a), McDougall and Taylor (1984), and Taylor and Buchens (1989). Analytical models of Stern (1976) and Howard and Veronis (1987) obtain $R_f = 0.25$ whereas results from other models (Schmitt, 1979b; Kunze, 1987) are centered around 0.6, which is more consistent with laboratory measurements.

The flux ratio in the present experiment at mid-depth is calculated and illustrated in Figure 13. The flux ratio quickly reaches a statistical mean around approximately $R_f \approx 0.55$ and maintains that value throughout the rest of the integration. Since this system does not correspond to the heat-salt system, it is not possible to make any comparisons with the laboratory experiments. However, Schmitt (1983) prepares maps of R_f as functions of Pr, R_ρ and K_T/K_S by employing an analytical model (Schmitt, 1979b) to be applied to the characteristics of fingers in a variety of fluid systems. Here, these formulae are employed to calculate a theoretical estimate of the flux ratio for the present double-diffusive system. It is worth noting that the actual density ratio increases during the integration from 1.6 at the beginning to 5.2 at the end of the integration (Fig. 9e). Within this range of density ratios, the analytical model yields R_f ranging from approximately 0.61 to 0.64 (i.e., with $Pr = 100$, $K_T/K_S = 30$). Considering the assumptions of the analytical model, there appears to be an approximate agreement of the value of the flux ratio in the present numerical experiment with this theoretical estimate.

Finally, the model fluxes are compared with the '⅓-flux law.' Based on dimensional grounds, Turner (1967) argues that the salt flux via salt fingers is proportional to the ⅓rd power of the salinity difference across the interface. In dimensional form, the salinity flux

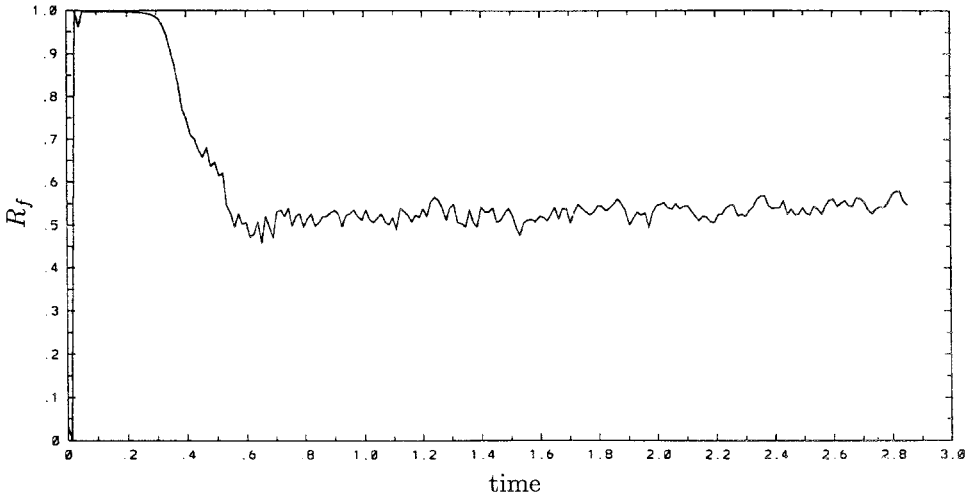

Figure 13. Flux ratio R_f along the mid-depth of the finger zone ($z = 0.75$) versus time .

law can be written as (Shen, 1993): $\beta\langle wS'\rangle = c(g\nu)^{1/3}\,(\beta\,\delta S)^{4/3}$, which after nondimensionalization becomes:

$$F_S = c\left(\frac{Ra}{Pr\,R_\rho}\right)^{1/3}(\delta S)^{4/3} \tag{11}$$

where δS is the salinity difference between the layers, and c is a constant.

The scatter diagram of F_S versus δS for the present experiment is shown in Figure 14 for

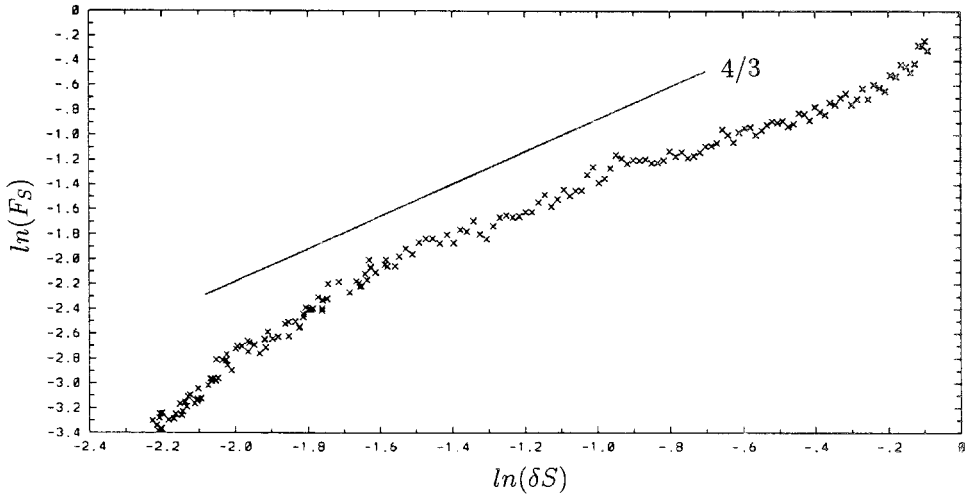

Figure 14. Scatter plot of F_S (nondimensional) versus S-stuff difference δS across the finger interface for $t > 0.5$.

$t > 0.5$ (i.e., after fingers develop). The slope of the solid line is equal to 4/3. While there is an approximate agreement with the 4/3 law over most of the integration time, the experimental slope exhibits deviations from 4/3 at high and low values of δS. High δS values (at the right end of the graph) correspond to the initial phase when the finger interface is thick and the mixed layers have not established yet. Low δS values (at the left end of the graph) correspond to the run-down phase when the layered structure starts to disintegrate. It is therefore reasonable to assume that the 4/3 law, which is derived based on the assumption of two distinct reservoirs, does not apply in these phases.

5. Discussion

Let us consider the energetics of an idealized system. The system evolves from a linear stratification (state 1) to a layered state (state 2) as shown in Figure 15a. The density distribution of the initial state is

$$\frac{\rho_1}{\rho_0} = \frac{1}{2} - \frac{z}{L_z}, \tag{12}$$

and the density distribution of state 2 is

$$\frac{\rho_2}{\rho_0} = \begin{cases} \frac{1}{2} + \Delta\rho & \text{for} \quad -\frac{L_z}{2} \le z \le -\frac{h}{2} \\ \frac{1}{2} - 2\Delta\rho\frac{z}{h} & \text{for} \quad -\frac{h}{2} \le z \le \frac{h}{2} \\ \frac{1}{2} - \Delta\rho & \text{for} \quad \frac{h}{2} \le z \le \frac{Lz}{2} \end{cases} \tag{13}$$

where ρ_0 is a reference density and $2\rho_0\,\Delta\rho$ is the density difference between the layers.

The following energy conservation statement can be written: $PE_1 - PE_2 = KE_2 + D$, where PE is the potential energy, KE is the kinetic energy, and D denotes the total energy loss to dissipation between states 1 and 2. The potential energy at state 1 becomes $PE_1 = -1/12\ g\ \rho_0\ L_z^2$ and the potential energy at state 2 is $PE_2 = -g\ \rho_0\ L_z^2\ \Delta\rho/4\ [1 - (h^2/L_z^2/3)]$. From the above expressions, we get an equation that describes the evolution of the interface:

$$\eta = \sqrt{3 - \frac{1 + 6B}{\Delta\rho}}, \tag{14}$$

where $\eta = h/L_z$ measures the interface thickness, and $B = (KE_2 + D)/(\frac{1}{2}g\rho_0 L_z^2)$ is the kinetic energy and dissipation normalized by the initial potential energy scale. Figure 15b shows η as a function of A for different density differences between the layers. Eq. (14) requires that $\Delta\rho \ge 1/3$ (the upper bound is: $\Delta\rho \le 1/2$), since otherwise the center of mass is raised from state 1 to state 2, and external energy input is necessary. Increasing B (i.e., high

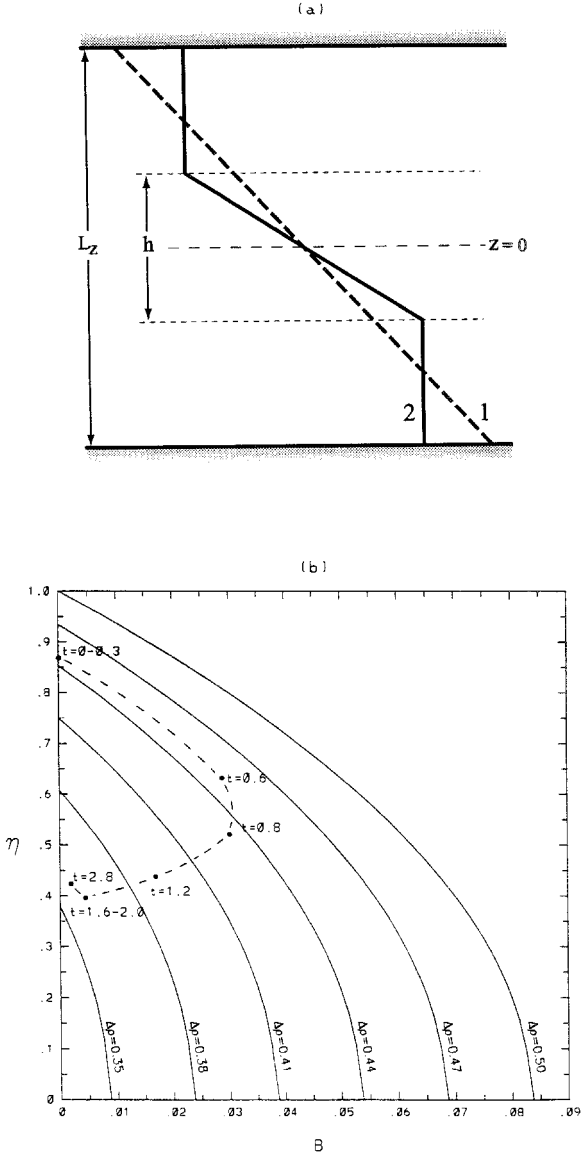

Figure 15. (a) The density distribution of an idealized system in a uniformly stratified and layered state. (b) The dependence of the interface thickness η on parameter B for different values of Δρ. The dashed line shows time-evolution of the present simulation.

kinetic energy or small domain size) while keeping Δρ constant leads to a smaller interface thickness. Along lines of constant B, the interface thickness decreases as Δρ decreases. Along lines of constant η, this graph implies that higher values of B correspond to larger density differences between the layers. These statements appear to be consistent with the dynamics of the present system.

The evolution of the interface thickness and density difference are plotted in Figure 15b for the present numerical simulation. (The contributions from the initial narrow zones at the top and bottom of the domain are neglected.) The path displays the generation of kinetic energy during the first part of Phase II ($0.3 < t < 0.8$), and the reduction of the thickness of the finger zone (see also Fig. 3). In the second half of Phase II ($0.8 < t < 1.2$), the kinetic energy in the system decreases, while the density difference between layers is also reduced due to exchange of properties via finger activity. In Phase III, the interface thickness remains roughly constant, while the density difference and kinetic energy continue to decrease. Phase IV exhibits some expansion of the interface along the line of approximately constant $\Delta\rho$ while kinetic energy keeps decreasing. The behavior of parameter B is similar to the evolution of kinetic energy (Fig. 8).

In this discussion, the fingers are only implicitly represented and act to convert the available potential energy into kinetic energy, hence purely as a mechanism to drive the convective cells in the mixed layers and to exchange properties in the vertical. The formation of layers is a result of these processes. Different double-diffusive systems will follow different paths in Figure 15b, as finger processes will develop different kinetic energy and density differences between the layers, depending on the parameters of the physical system (i.e., Pr, Sc, Ra and R_ρ).

The horizontal boundaries in this system play an important role in the development of the layered state. At the top and bottom boundaries, light and heavy finger fluxes accumulate what leads to the formation of mixed layers. Increasing the vertical extent of the domain will alter the quasi-equilibrium configuration reached by the system. This is supported by the above analysis which shows dependence of parameter B characterizing the system on L_z.

The above consideration does not provide an equilibrium thickness for the finger interface. It has been assumed since the collective instability work by Stern (1969) that the vertical integrity of the finger column is related to the thickness of the finger zone. This theory implies that initially the gradient zone is large such that individual fingers cannot extend across it. After the fingers start penetrating through the interface, they effectively transport fluid from the lower reservoir into the upper reservoir, and vice versa. When many fingers are present, an equilibrium interface thickness is maintained in the statistical sense, as long as potential energy is available. However, this explanation is not entirely supported by the present numerical simulation. The fingers are quite disordered and do not form columns across the interface during the quasi-equilibrium state (Fig. 7). While they are still elongated in the vertical direction, their amplitudes appear to be smaller than the thickness of the interface. Despite the irregular finger structure, a layered state is maintained in a quasi-equilibrium (Phase III).

6. Summary and conclusions

In this paper, the evolution of fingers in a double-diffusive system is investigated using numerical integration of two-dimensional equations of motion for an incompressible, Boussinesq fluid. The computational domain is closed in vertical with no-flux boundary

conditions and periodic in horizontal. The system is initialized with linear stratifications for both fast and slow diffusing components. The major result of this study is the appearance of a quasi-equilibrium state characterized by a finger interface in between two mixed layers exhibiting larger-scale convection cells. At the zero-flux top and bottom boundaries, light and heavy finger fluxes accumulate what leads to the formation of mixed layers, which gradually grow and erode away the vertical density stratification. The mixed layers and the finger interface reach a quasi-equilibrium state, which is maintained until the fingering motion and the convective cells weaken, and the vertical diffusion of T leads to the expansion of the interface.

It has been generally assumed that the finger zone in an equilibrium state consists of columns of fingers whose amplitude is equal to the thickness of the finger zone. However, the numerical result presented here contradicts this notion. In the quasi-equilibrium state, the fingers within the finger interface are quite irregular and do not extend throughout the entire region, even though the Stern number is below the critical value. Some theories of finger instability (Holyer, 1984; Howard and Veronis, 1992) show that the fingers are intrinsically unstable virtually at all scales. Broken, wiggly fingers are also observed in laboratory experiments (Taylor and Buchens, 1989; Taylor and Veronis, 1996). Taylor (1993) calculates from laboratory experiments that the average ratio of the width to the length of unsheared heat-salt fingers is 0.58 (for $R_\rho < 5$). The investigation of this behavior is of interest considering that the oceanic interfaces are typically several meters thick.

Once the nature of the interaction between the finger zone and mixed layers is understood in more detail, one may tackle other important issues, such as the spontaneous formation of multiple interfaces from constant T and S gradients.

Acknowledgments. The authors wish to thank R. W. Schmitt, M. Stern and C. Rooth for constructive discussions. Two anonymous reviewers helped to improve the manuscript greatly. We also thank B. Cushman-Roisin and E. P. Chassignet for their support and contribution during earlier stages of this study. T. M. Özgökmen was supported by the Rosentiel Postdoctoral Fellowship, O. E. Esenkov and D. B. Olson were supported by the National Science Foundation under grant OCE-93-14447.

REFERENCES

Arakawa, A. 1966. Computational design for long-term numerical integration of the equations of fluid motion: Two dimensional incompressible flow. Part I. J. Comput. Phys., *1,* 119–143.

Gazdag, J. 1976. Time-differencing schemes and transform methods. J. Comput. Phys., *20,* 196–207.

Griffiths, R. W. and B. R. Ruddick. 1980. Accurate fluxes across a salt-sugar finger interface deduced from direct density measurements. J. Fluid Mech., *99,* 85–95.

Herring, J. R., S. A. Orszag, R. H. Kraichnan and D. G. Fox. 1974. Decay of two-dimensional homogeneous turbulence. J. Fluid Mech., *66,* 417–444.

Holyer, J. Y. 1981. On the collective instability of salt fingers. J. Fluid Mech., *110,* 195–207.

—— 1984. The stability of long, steady, two-dimensional salt fingers. J. Fluid Mech., *147,* 169–185.

Howard, L. N. and G. Veronis. 1987. The salt-finger zone. J. Fluid Mech., *183,* 1–23.

—— 1992. Stability of salt fingers with negligible diffusivity. J. Fluid Mech., *239,* 511–522.

Kunze, E. 1987. Limits on growing, finite-length salt fingers: A Richardson number constraint. J. Mar. Res., *45,* 533–556.

Lambert, R. B. and J. W. Demenkow. 1972. On the vertical transport due to fingers in double-diffusive convection. J. Fluid Mech., *54,* 627–640.

Linden, P. F. 1973. On the structure of salt fingers. Deep-Sea Res., *20,* 325–340.

McDougall, T. J. and J. R. Taylor. 1984. Flux measurements across a finger interface at low values of the stability ratio. J. Mar. Res., *42,* 1–14.

Marmorino, G. O. 1987. Observations of small-scale mixing processes in the seasonal thermocline. Part I: Salt fingering. J. Phys. Oceanogr., *17,* 1339–1347.

Piacsek, S. and J. Toomre. 1980. Nonlinear evolution and structure of salt fingers. Marine Turbulence, *28,* 193–219.

Schmitt, R. W. 1979a. Flux measurements at an interface. J. Mar. Res., *37,* 419–436.

—— 1979b. The growth rate of super-critical fingers. Deep-Sea Res., *26,* 23–40.

—— 1981. Form of the temperature-salinity relationship in the Central Water: evidence for double-diffusive mixing. J. Phys. Oceanogr., *11,* 1015–1026.

—— 1983. Characteristics of salt fingers in a variety of fluid systems including stellar interiors, liquid metals, oceans, and magmas. Phys. Fluids, *26,* 2373–2377.

Schmitt, R. W. and D. T. Georgi. 1982. Finestructure and microstructure in the North Atlantic Current. J. Mar. Res., *40* (Suppl.), 659–705.

Schmitt, R. W., H. Perkins, J. D. Boyd and M. C. Stalcup. 1987. C-SALT: an investigation of the thermohaline staircase in the western tropical North Atlantic. Deep-Sea Res., *34,* 1697–1704.

Shen, C. Y. 1989. The evolution of the double-diffusive instability: Salt fingers. Phys. Fluids, *A1,* 829–844.

—— 1993. Heat-salt finger fluxes across a density interface. Phys. Fluids, *A5,* 2633–2643.

Shen, C. Y. and G. Veronis. 1997. Numerical simulation of two-dimensional fingers. J. Geophys. Res., *102,* 23131–23143.

Stern, M. E. 1960. The "salt fountain" and thermohaline convection. Tellus, *12,* 172–175.

—— 1969. Collective instability of salt fingers. J. Fluid Mech., *35,* 209–218.

—— 1975. Ocean Circulation Physics, cp. XI, Academic, 196–200.

—— 1976. Maximum buoyancy flux across a salt finger interface. J. Mar. Res., *34,* 95–110.

Stern, M. E. and J. S. Turner. 1969. Salt fingers and convecting layers. Deep-Sea Res., *16,* 497–511.

Swarztrauber, P. N. 1977. The methods of cyclic reduction, Fourier analysis and FACR algorithm for discrete solution of the Poisson equation on a rectangle. SIAM Rev., *19,* 490–501.

Taylor, J. R. 1993. Anisotropy of salt fingers. J. Phys. Oceanogr., *23,* 554–565.

Taylor, J. R. and G. Veronis. 1996. Experiments on double-diffusive sugar-salt fingers at high stability ratio. J. Fluid Mech., *321,* 315–333.

Taylor, J. R. and P. Buchens. 1989. Laboratory experiments on the structure of salt fingers. Deep-Sea Res., *36,* 1675–1704.

Turner, J. S. 1967. Salt fingers across a density interface. Deep-Sea Res., *14,* 599–611.

—— 1985. Multicomponent convection. Ann. Rev. Fluid Mech., *17,* 11–44.

Whitfield, D. W. A., G. Holloway and J. Y. Holyer. 1989. Spectral transform simulations of finite amplitude double-diffusive instabilities in two dimensions. J. Mar. Res., *47,* 241–265.

Williams, A. J. 1974. Salt fingers observed in the Mediterranean outflow. Science, *185,* 941–943.

Received: *5 December, 1996;* revised: *20 November, 1997.*